

COMPARISON OF CONVENTIONAL AND ACCELERATED 4D FLOW MRI ON A FLOW PHANTOM

Morgane Garreau^{1,2}, Thomas Puiseux^{2,3}, Ramiro Moreno^{3,4}, Solenn Toupin⁵, Daniel Giese⁶, Simon Mendez¹, and Franck Nicoud¹

¹IMAG, Univ. Montpellier, CNRS UMR 5149, Montpellier, France, ²Spin Up, Toulouse, France, ³I2MC, INSERM/UPS UMR 1297, Toulouse, France, ⁴ALAR Expertise, Strasbourg, France, ⁵Siemens Healthcare France, Saint-Denis, France, ⁶Siemens Healthcare, Erlangen, Germany

Synopsis

Fully-sampled and accelerated (GRAPPA R=3 and compressed sensing R=7.6) 4D Flow MRI acquisitions were compared for velocity profiles, flow rates and peak velocities in a rigid cardiovascular phantom under complex pulsatile flow conditions. Compatible CFD simulations were performed under the same flow conditions as a complementary modality. Good agreement was found between the three MR techniques, but discrepancies relative to the principle of mass conservation were noticed. Even though CFD presents some limitations as well, it appears to be a useful tool to investigate these differences.

INTRODUCTION

Time-resolved 3D phase-contrast (PC) MRI, also called 4D flow MRI, is a promising technique to retrospectively evaluate flows inside a 3D volume. Thereby hemodynamic parameters such as peak velocity and flow rates, along with derived biomarkers, e.g., wall shear stress, turbulent kinetic energy, become accessible in a non-invasive way¹. However, its development in clinical routine remains limited by the long scan times. To decrease the scan duration, techniques like parallel imaging have been developed. In this study, two acceleration methods, GRAPPA (R=3) and compressed sensing (R=7.6), were investigated together with a fully-sampled k-space 4D flow acquisition. The experiment was conducted in a well-controlled setup under pulsatile inflow regime presenting complex flow features characteristic of the cardiovascular system. A Computational Fluid Dynamics (CFD) simulation was also performed under the same conditions and used as a third-party reference to characterize the differences.

METHODS

The rigid phantom setup used to acquire the 4D flow MRI data is presented in the coronal (xz)-plane in Figure 1. The circuit was supplied with a Newtonian blood-mimicking fluid following a sinusoidal pulsatile flow rate imposed at the phantom inlet. The investigated acquisition methods were a complete k-space sampling (fully-sampled, FS), GRAPPA R=3 (G3) and compressed sensing (CS, prototypal sequence) R=7.6 at 1.5 T (MAGNETOM Sola, Siemens Healthcare, Erlangen, Germany). Isotropic 2mm³ voxels were set with TE=3.70-4.15 ms, temporal resolution =48.3-51.8 ms, simulated cardiac R-R interval =1 s, 20 (FS, G3) or 25 (CS) reconstructed cardiac phases and encoding velocities (VENC) =0.7 m/s in-plane and 0.2 m/s through-plane. All MR images went through an in-house post-processing procedure to correct for through-plane geometric distortion, noise masking and phase unwrapping.

CFD simulation was conducted using the YALES2BIO solver (<https://imag.umontpellier.fr/~yales2bio/>) on the same computer-aided design (CAD) geometry². The velocity at the inlet boundary was prescribed from 2D cine PC-MRI measurements. In order to compare both techniques, the CFD velocity fields were phase-averaged and downsampled to the MRI spatial resolution³. These low-resolution fields are referred to as CFD,LR. Finally, MRI volumes were registered onto the computational model.

RESULTS

Scan times for FS, G3 and CS were 42:40, 14:40 and 5:35 min respectively. As displayed in Figure 2, the main flow structures were well captured by the different modalities at peak systole (highest flow rate at the inlet), as well as end diastole (lowest flow rate).

However, higher velocities can be observed for MRI as compared to CFD in the collateral canal and at the junction with the descending main pipe. To better appreciate the discrepancies, the normal velocity profiles are reported in Figure 3 at four locations of interest (see Figure 1).

Good agreement was found between all MRI modalities, except for FS at peak systole in the collateral where higher normal velocities are recorded. Good agreement with CFD,LR was also found for low velocities. However, the values reported by CFD in the collateral and at peak diastole in the junction are lower in magnitude and the profiles appear shifted.

Concerning flow rates as displayed in Figure 4 (a), similar patterns were observed for the different MRI acquisitions, although the principle of mass conservation appears not to be met, especially in the aneurysm-like section and between the ascending and descending main pipes. At peak diastole, the average flow rates (in mL, reported as mean \pm SD) respectively for FS, G3, CS and CFD,LR were found to be 105.2 ± 3.4 , 105.6 ± 4.5 , 104.0 ± 4.0 and 92.2 ± 0.1 in the upper part of the phantom and 56.4 ± 10.9 , 57.9 ± 12.9 , 52.1 ± 12.8 and 64.0 ± 0.2 in the collateral duct. At end diastole, the following values were reported: on the one hand 39.3 ± 2.9 , 39.3 ± 4.3 , 37.2 ± 3.8 and 36.5 ± 0.0 , and on the other hand -59.6 ± 8.4 , -57.7 ± 6.0 , -64.6 ± 13.2 and -49.4 ± 0.2 . The peak velocities along the same paths as the flow rates are presented in Figure 4 (b) and were computed only on voxels entirely inside the phantom volume to avoid noise due to partial volume effects. In a global manner, these velocities were equal or higher for MR acquisitions compared to the ones found for the CFD simulations, for which mass is conserved.

DISCUSSION

Velocity profiles, flow rates and peak velocities were investigated under the same flow conditions for a fully-sampled MR acquisition, as well as two acceleration techniques: GRAPPA and compressed sensing. Contrarily to what was previously observed⁴, the results were comparable for all three techniques, suggesting that compressed sensing is a suitable modality to perform fast 4D flow acquisitions. However, mass appears not to be conserved, especially in the aneurysm-like region, where highly disturbed flow patterns occur. Furthermore, the sections where the MR velocity profiles deviate from the ones simulated by the CFD correspond to locations associated with high flow velocity or acceleration.

These discrepancies can most probably be related to spatial and velocity displacement artifacts⁵. MR globally overestimates the flow rates compared to CFD. Future work could include investigating more physiological flow rates waveforms, implementing post-processing methods to compensate the previously mentioned artifacts⁶ or simulating 4D flow MRI to further characterize the observed divergences⁷.

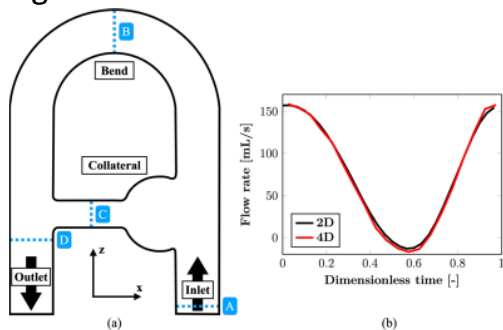
Acknowledgements

No acknowledgement found.

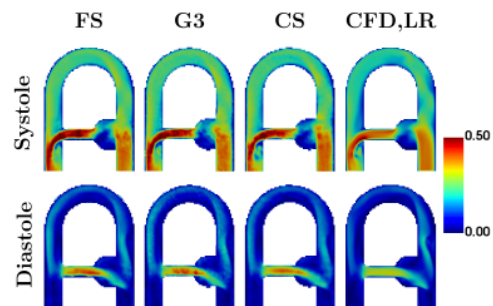
References

1. Stankovic Z, Allen BD, Garcia J, Jarvis KB, Markl M. 4D flow imaging with MRI. *Cardiovasc Diagn Ther.* 2014;4(2):173-192.
2. Mendez S, Chnafa C, Gibaud E, Sigüenza J, Moureau V, Nicoud F. YALES2BIO: A computational fluid dynamics software dedicated to the prediction of blood flows in biomedical devices. In: IFMBE Proceedings. Springer International Publishing; 2015:7-10.
3. Puiseux T, Sewonu A, Meyrignac O, et al. Reconciling PC-MRI and CFD: An in-vitro study. *NMR Biomed.* 2019;32(5):e4063.
4. Pathrose A, Ma L, Berhane H, et al. Highly accelerated aortic 4D flow MRI using compressed sensing: Performance at different acceleration factors in patients with aortic disease. *Magn Reson Med.* 2021;85(4):2174-2187.
5. Steinman DA, Ethier CR, Rutt BK. Combined analysis of spatial and velocity displacement artifacts in phase contrast measurements of complex flows. *J Magn Reson Imaging.* 1997;7(2):339-346.
6. Thunberg P, Wigström L, Wranne B, Engvall J, Karlsson M. Correction for acceleration-induced displacement artifacts in phase contrast imaging. *Magn Reson Med.* 2000;43(5):734-738.
7. Puiseux T, Sewonu A, Moreno R, Mendez S, Nicoud F. Numerical simulation of time-resolved 3D phase-contrast magnetic resonance imaging. *PLoS One.* 2021;16(3):e0248816.

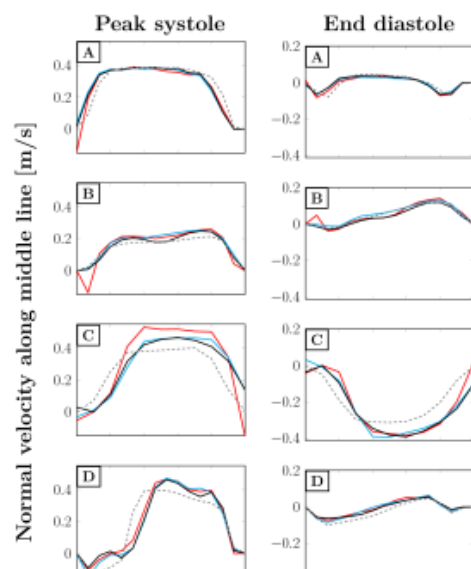
Figures



(a) Flow phantom schematic representation in the coronal plane. The dotted lines indicate locations of interest, along which velocity profiles were analyzed. (b) Inlet flow rate over time recorded for the fully-sampled 4D Flow acquisition (red) and 2D cine PC-MRI used as CFD boundary condition (black).



Velocity magnitude fields at peak systole (above) and end diastole (below) for the MR acquisitions and the CFD simulation.

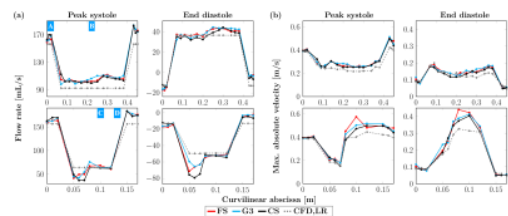




Normalized line length [-]

— FS — G3 — CS ... CFD,LR

Normal velocity profiles along the lines indicated in Figure 1 (A: inlet, B: bend, C: middle of collateral, D: junction of collateral and main branch) at peak systole and end diastole.



(a) Flow rate and (b) Peak velocities at peak systole and end diastole. The curvilinear abscissa on the horizontal axes correspond to paths going respectively through the main duct for the figures above and through the collateral for the figures below, from the inlet to the outlet. For all figures, the three first positions correspond to planes before the bifurcation of the main and collateral ducts and the three last ones to planes after the junction of these two conduits. The letters A-D refer to the plane locations given in Figure 1.